

# Towards Magnon Valleytronics

Doried Ghader

College of Engineering and Technology, American University of the Middle East, Kuwait

Valleytronics is a pioneering technological field relying on the valley degree of freedom to achieve novel electronic functionality. Topological valley-polarized electrons confined to domain walls in bilayer graphene were extensively studied in view of their potentials in valleytronics. Here, we study the magnonic version of domain wall excitations in 2D honeycomb ferromagnetic bilayers (FBL). We report new topological phases in these materials, determined by Dzyaloshinskii-Moriya interaction, electrostatic doping, and interlayer exchange. We further demonstrate that layer stacking domain walls in FBL can be used as 1D channels for ballistic transport of topological valley-polarized magnons. Our theoretical results raise hope towards magnon valleytronics based on atomically thin topological magnetic materials.

**Introduction.** The recent realization of two-dimensional (2D) materials with intrinsic magnetism [1, 2] constituted an important breakthrough in condensed matter physics. This discovery immediately stimulated tremendous interest in the fundamental physics underlying 2D magnets, as well as their technological potentials [3-22]. With the novel characteristics of their magnetic excitations, 2D magnets are expected to open new horizons in technological fields like magnonics. The magnon spectrum in 2D monolayer honeycomb ferromagnets mimics the electronic band structure of graphene [11], with degenerate bands at the non-equivalent valleys  $K$  and  $K' = -K$  (Fig. 1a). The energy degeneracy at the valleys is protected by inversion and time reversal symmetries. Next-nearest-neighbor Dzyaloshinskii-Moriya interaction (DMI), present in several 2D ferromagnets, breaks the time-reversal symmetry [5] and opens topological gaps at  $\pm K$  (Fig. 1b). Similar to monolayers, bilayer ferromagnets exhibit a pair of degenerate bands at the inequivalent valleys. Valley gaps in ferromagnetic bilayers (FBL) can be induced by intralayer DMI [6, 9] (Figs. 2c) or by breaking the inversion symmetry through layer-dependent electrostatic doping [23, 24] (Figs. 2d). In a recent theoretical study [24], AB-stacked FBL gapped by electrostatic doping is predicted to be a topological insulating phase, featuring topological magnon valley currents and valley Hall effect. This novel behavior of magnetic excitations in gapped FBL is guaranteed by the non-trivial Berry curvatures of valley magnons and the no-valley mixing symmetry.

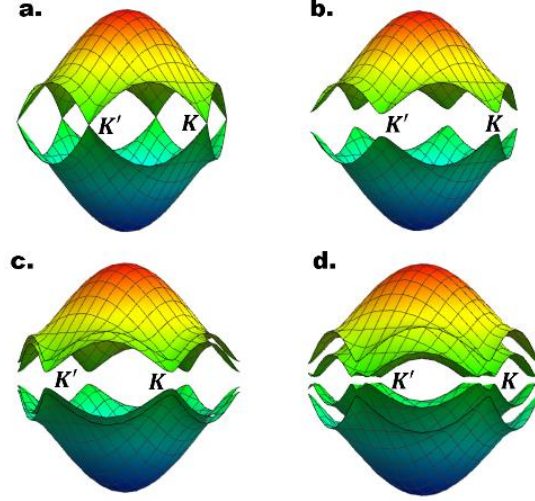


**Figure 1:** (a) and (b) Gapless magnon spectrum and DMI induce gap in monolayer honeycomb ferromagnet. (c) and (d) illustrate the gapped FBL magnon spectrum due to intralayer DMI and layer-dependent electrostatic doping respectively.

The valley degree of freedom in electronic systems is proved very promising for quantum technologies, leading to the novel technological field of valleytronics [25–38]. In particular, topological confinement of electronic states on domain walls of bilayer graphene (BLG) has been successfully proposed to realize novel nano-electronic devices, including valley filters, valley valves, and field effect transistors. Applying a perpendicular electric field in BLG breaks inversion symmetry and consequently opens a (valley) band gap that admits a topological interpretation [26, 39-46]. The applied field induces a non-trivial Berry curvature for the low energy valence band, with opposite signs near the two valleys. Although the Chern number  $N$  over the full Brillouin zone (BZ) vanishes, the Berry curvature integral  $N_v$  within a single valley  $v$  is nonzero [26, 27, 47-51]. The valley indices  $N_v$  in gapped BLG are interpreted as “valley Chern numbers”, converging to quantized values  $N_v = \pm 1$  for nonequivalent valleys. Novel domain walls can then be formed by a sign reversal of the perpendicular electric field, which flips the sign of  $N_v$ . Across the electric-field domain wall (EFW), the valley Chern number hence changes by  $\Delta N_v = \pm 2$ , where  $\Delta N_v$  represents a well-defined topological invariant [47]. In agreement with the bulk-edge correspondence,  $\Delta N_v$  is associated with the appearance of a pair of valley-polarized chiral electrons confined to the EFW [26, 47]. Domain walls can also be formed in BLG by interlayer stacking reversal, where the layer stacking switches from AB to BA configurations. In the presence of a uniform interlayer electric field, layer stacking domain walls (LSW) also support pairs of topological chiral modes [27, 33, 52], interpreted also in terms of the sign reversal of the integer valley Chern number.

The technological interest in the valley degree of freedom was extended to 2D photonic [53] and phononic [54] crystals. Magnon valleytronics, however, did not yet receive the deserved attention.

The realization of magnon valleytronic devices demands novel magnetic materials where magnons with preserved valley index can ballistically propagate with lowest dissipation. In this work, we propose topological LSW in 2D FBL as a promising candidate for this end. We first investigate new topological phases in FBL with uniform layer-dependent electrostatic doping (ED) and weak DMI, followed by an analysis of valley-polarized magnons confined to LSW.

**Four-band formalism.** With nearest neighbor exchange, DMI and electrostatic doping, the full BZ Hamiltonian for magnons in AB-stacked FBL reads [6, 9, 24],

$$\mathcal{H}_{AB} = JS \begin{pmatrix} (3+U)I + \mathcal{H}_1 & \mathcal{H}_3 \\ \mathcal{H}_3^\dagger & (3-U)I + \mathcal{H}_2 \end{pmatrix}$$

with  $\mathcal{H}_1 = \begin{pmatrix} f_D(\vec{p}) + v_0 & -f(\vec{p}) \\ -f^*(\vec{p}) & -f_D(\vec{p}) \end{pmatrix}$ ,  $\mathcal{H}_2 = \begin{pmatrix} f_D(\vec{p}) & -f(\vec{p}) \\ -f^*(\vec{p}) & -f_D(\vec{p}) + v_0 \end{pmatrix}$ ,  $\mathcal{H}_3 = \begin{pmatrix} 0 & -v_0 \\ 0 & 0 \end{pmatrix}$  and  $I$  is the  $2 \times 2$  identity matrix. The exchange and DMI lattice functions are  $f(\vec{p}) = e^{\frac{ip_y}{\sqrt{3}}} + 2e^{-\frac{ip_y}{2\sqrt{3}}} \cos(p_x/2)$  and  $f_D(\vec{p}) = (D/J)[4\cos(\sqrt{3}p_y/2)\sin(p_x/2) - 2\sin(p_x)]$ . The parameter  $v_0 = J_\perp/J$ , where  $J$  and  $J_\perp$  denote the nearest neighbor intra and interlayer exchange coefficients respectively.  $S$  denotes spin,  $D$  is the DMI coefficient, and  $U$  represents the layer-dependent electrostatic doping potential (normalized by  $JS$ ).  $p_x$  and  $p_y$  are the momenta along  $x$  and  $y$  directions. The BA-configuration Hamiltonian  $\mathcal{H}_{BA}$  can be deduced easily.

Note that these magnonic Hamiltonians do not have identical electronic analogues. The full BZ Hamiltonians will allow us to calculate the bulk magnon bands, their Berry curvatures and Chern numbers, as well as the magnon thermal Hall and Nernst conductivities.

Expanding  $\mathcal{H}_{AB}$  near  $\pm K$  valleys yields the Dirac Hamiltonians  $\mathcal{H}_{AB}^K = \tau_0(3\sigma_0 + m\sigma_z + \frac{\sqrt{3}}{2}\vec{p} \cdot \vec{\sigma}) + U\tau_z\sigma_0 + v_0\Gamma_{AB}$  and  $\mathcal{H}_{AB}^{-K} = \tau_0(3\sigma_0 + m\sigma_z - \frac{\sqrt{3}}{2}\vec{p} \cdot \vec{\sigma}^*) + U\tau_z\sigma_0 + v_0\Gamma_{AB}$ . We defined the DMI parameter  $m = 3\sqrt{3}D/J$ . The Pauli matrices  $\sigma$  and  $\tau$  correspond to the sublattice and layer spaces respectively. The matrix  $\Gamma_{AB} = \frac{1}{2}(\tau_z\sigma_z + \tau_0\sigma_0) - \frac{1}{4}(\tau_+\sigma_+ + \tau_-\sigma_-)$ , and for BA-stacking,  $\Gamma_{AB}$  is replaced by  $\Gamma_{BA} = \frac{1}{2}(-\tau_z\sigma_z + \tau_0\sigma_0) - \frac{1}{4}(\tau_+\sigma_- + \tau_-\sigma_+)$ .

We next consider a 2D FBL with LSW (at  $x = 0$ ), separating two regions with AB and BA stacking in the domains  $x > 0$  and  $x < 0$  respectively. The corresponding four-components magnon wavefunctions in the regions  $x \gtrless 0$  are denoted  $\psi^\pm$  respectively, with  $\psi^\pm = \{\phi_i^\pm, i = 1, \dots, 4\}$ . The translational symmetry in the system is broken (preserved) along the  $x$  – direction ( $y$  – direction). The behavior of  $\psi^\pm$  is hence dictated by the functional form  $e^{-\lambda x} e^{ip_y}$ , where

$\lambda = \alpha + i\beta$  denotes the generalized phase factor in the  $x$  – direction [15, 18, 20, 21, 26, 27]. For intragap modes confined to the LSW,  $\lambda$  is real and the wavefunction decays exponentially away from the LSW.

Reinstating the momenta as differential operators in  $\mathcal{H}_{AB}^{\pm K}$  (equivalently  $\mathcal{H}_{BA}^{\pm K}$ ), the wave equation  $(\mathcal{H}_{AB}^{\pm K} - \epsilon I)\psi = 0$  yields four real solutions for  $\lambda$ , namely

$$\lambda_{1(2)}^{\pm} = \pm \sqrt{p_y^2 - \frac{a + (-)b}{v^2}}$$

with

$$a = 9 - m^2 + \Omega^2 + 3v_0 - \Omega(6 + v_0) + U^2$$

$$b = \sqrt{(-3 + \Omega)[(-3 + \Omega)v_0^2 + 4(-3 + \Omega)U^2 - 4v_0U(m + U)]}$$

and  $\Omega = \frac{\epsilon}{JS}$ . The solutions  $\lambda^{\pm}$  are adopted for  $\psi^{\pm}$  respectively, which gives  $\phi_i^{\pm} = u_{i1}e^{-\lambda_1^{\pm}x}e^{ip_y} + u_{i2}e^{-\lambda_2^{\pm}x}e^{ip_y}$ . The four-band formalism hence generates 16 coefficients  $\{u_{ij}; i = 1, . . 4, j = 1, 2\}$ , to be determined via boundary conditions derived using the matching method [26, 27, 55-59]. To be specific, the boundary conditions are derived by matching the wavefunctions components  $\phi_i^{\pm}$  and their derivatives across the LSW. First, the magnon wavefunction is required to be continuous across the domain wall, resulting in 4 boundary equations  $\phi_i^+(x = 0^+) = \phi_i^-(x = 0^-)$ . The remaining 12 boundary equations are derived by matching the rows of the wave equations  $(\mathcal{H}_{AB}^K - \epsilon I)\psi^> = 0$  and  $(\mathcal{H}_{AB}^K - \epsilon I)\psi^< = 0$  across the LSW. For example, considering the first row from each equation yields

$$v_0\phi_1^+ - iv(\partial_x\phi_2^+ - \partial_x\phi_2^-) - v_0\phi_4^+ = 0$$

$$(3 + U + m - \Omega)(\partial_x\phi_1^+ - \partial_x\phi_1^-) + v_0(\partial_x\phi_1^+ - \partial_x\phi_4^+) - ivp_y(\partial_x\phi_2^+ - \partial_x\phi_2^-) - iv(\partial_x^2\phi_2^+ - \partial_x^2\phi_2^-) = 0$$

$$(3 + U + m - \Omega)(\partial_x^2\phi_1^+ - \partial_x^2\phi_1^-) + v_0(\partial_x^2\phi_1^+ - \partial_x^2\phi_4^+) - ivp_y(\partial_x^2\phi_2^+ - \partial_x^2\phi_2^-) - iv(\partial_x^3\phi_2^+ - \partial_x^3\phi_2^-) = 0$$

The first equation is determined by subtracting the rows. Applying  $\partial_x$  and  $\partial_x^2$  followed by subtraction yields the second and third equation respectively.

With the boundary conditions in hand, we substitute  $\phi_i^\pm = u_{i1}e^{-\lambda_1^\pm x}e^{ip_y} + u_{i2}e^{-\lambda_2^\pm x}e^{ip_y}$  and deduce a  $16 \times 16$  linear system,  $M|u\rangle = 0$ . The determinant equation  $|M(p_y, \Omega)| = 0$  then yields the dispersion relations  $\Omega(p_y)$  for the intragap magnon modes confined to the LSW. We succeeded in reducing the determinant equation, which boils down to

$$(c_1\lambda_1^+ + c_2\lambda_2^+ + c_{12}\lambda_1^+\lambda_2^+ + c_0)(c_1\lambda_1^+ + c_2\lambda_2^+ - c_{12}\lambda_1^+\lambda_2^+ - c_0) = 0$$

with  $c_{1(2)} = vv_0[-9 + 3a + m^2 - U^2 - 2p_y^2v^2 - 6v_0 - (+)b - (+)\Omega(6 - e + 2v_0)]$  and  $c_{12} = v^2(2p_y^2v^2 - 2a)$ .

**Numerical results.** We will denote the 4 energy bands by  $[\epsilon_4, \epsilon_3, \epsilon_2, \epsilon_1]$ , arranged in descending energy order. Without ED, the DMI induces a non-trivial Berry curvature with 6-fold rotational symmetry for the four bands [6, 9]. The corresponding band Chern numbers are  $[0, -2, 0, 2]$ , which are independent of the exact value of DMI and interlayer exchange. Due to the 6-fold rotational symmetry, the  $\pm K$  valleys are topologically identical. Moreover, the magnon Berry curvatures are independent of the stacking, and the AB-BA domain walls do not confine magnon modes.

Introducing ED in the presence of DMI alters significantly the topology of the FBL and results in new topological phases. Figures 2a-2d present the AB-configuration Berry curvatures of conduction-like ( $\epsilon_3$ ) and valence-like ( $\epsilon_2$ ) bands for selected values of ED, DMI and interlayer exchange.

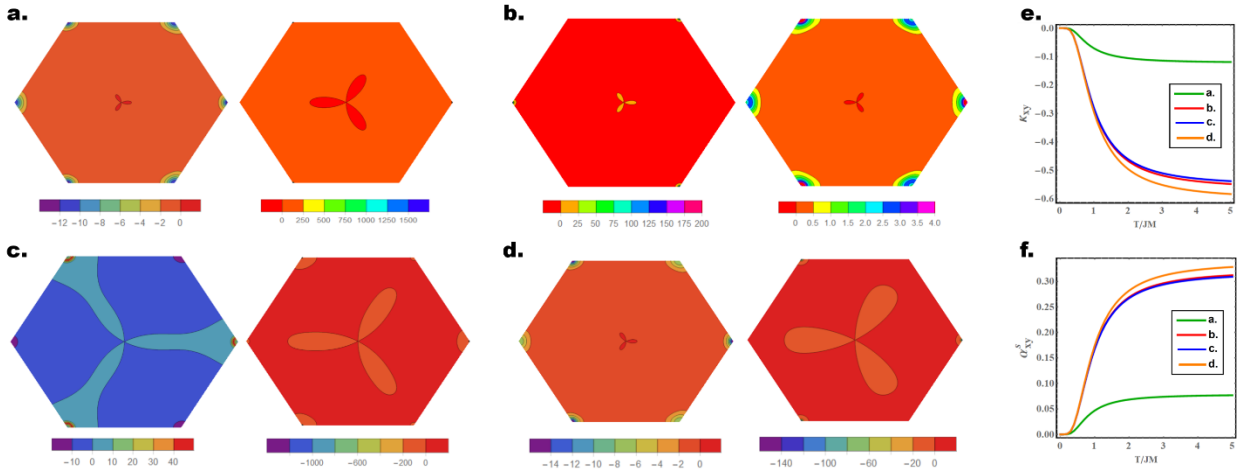


**Figure 2:** (a-d) Representative Berry curvatures for  $\epsilon_3$  (left) and  $\epsilon_2$  (right) bands in FBL with ED and DMI. The parameter choices are  $(U = 0.1, D = 0.05J, v_0 = 0.3)$ ,  $(U = 0.2, D = 0.05J, v_0 = 0.2)$ ,  $(U = 0.2, D = 0.02J, v_0 = 0.3)$ , and  $(U = 0.1, D = 0.05J, v_0 = 0.5)$  respectively. (e) and (f) present the temperature evolution of Hall ( $\kappa_{xy}$ ) and Nernst ( $\alpha_{xy}^S$ ) conductivities corresponding to the parameters in (a-d).

The Berry curvatures are calculated from the full BZ Hamiltonian  $\mathcal{H}_{AB}$  and using the numerical approach developed in reference [60]. Cases 2a-2c correspond to three new topological phases, with Chern numbers  $[-2,1,0,1]$ ,  $[-1,1,-1,1]$ , and  $[0,-1,0,1]$  respectively. Case 2d reproduces the ED-free topological phase with Chern numbers  $[0,-2,0,2]$ . Remarkably, the FBL topology depends on the specific values of  $U$ ,  $D$ , and the interlayer exchange parameter  $v_0$ . Further, figures 2a-2d illustrate the Berry curvature valley mixing in FBL with ED and DMI. Consequently, valley Chern numbers and Hall effect cannot be defined in these bilayers. Nevertheless, the non-trivial topology of the bands induces standard Hall and Nernst conductivities [3, 4, 6, 12, 17, 22] plotted in figure 2e for the 4 different topological phases of figures 2a-2d.

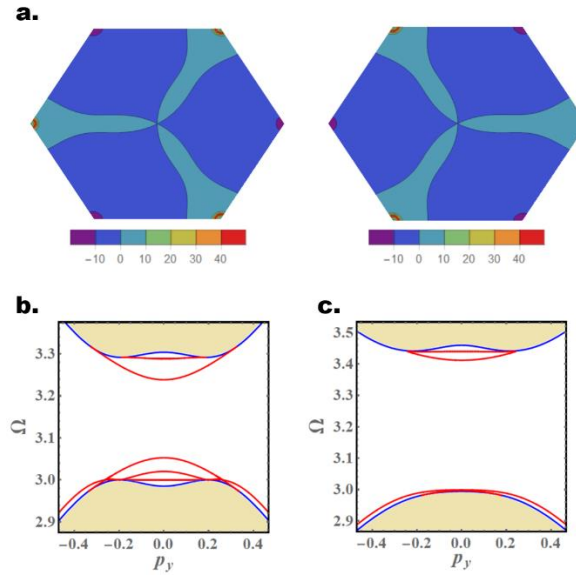


**Figure 3:** (a) Berry curvatures for the  $\epsilon_3$  band in AB (left) and BA (right) stacked FBL with parameters ( $U = 0.2, D = 0.02J, v_0 = 0.3$ ). (b) and (c) show the magnon bulk spectra (shaded regions) and domain wall magnon modes (red) near the  $K$ -valley for ( $U = 0.2, D = 0.02J, v_0 = 0.3$ ) and ( $U = 0.2, D = 0.05J, v_0 = 0.3$ ) respectively.

Another important consequence of ED is that it breaks inversion symmetry and hence the 6-fold rotational symmetry of the Berry curvatures. This gives relevance to the AB-BA domain walls in FBL with ED and DMI. As illustrated numerically in figure 3a, inverting the layer registry rotates the Berry curvatures by  $\pi/3$ . The LSW hence separates two regions with different Berry curvatures but identical Chern numbers. Although the LSW is topologically compensated, it can still host 1D magnon modes (figures 3b and 3c). Indeed, the localized magnon modes in the present case do not correspond to a topological invariant valley index, and the LSW spectrum is completely gapped near  $\pm K$  valleys. Despite some similarities with topologically compensated LSW in BLG with reversed gating and layer stacking [27], the present case is topologically different and does not have an identical fermionic analogue.

We now focus on FBL with ED and negligible DMI. Figure 4 illustrates the magnon Berry curvature profile for the valence-like band characterized by a broken 6-fold rotational symmetry and no valley mixing. A similar profile holds for the rest of the bands.

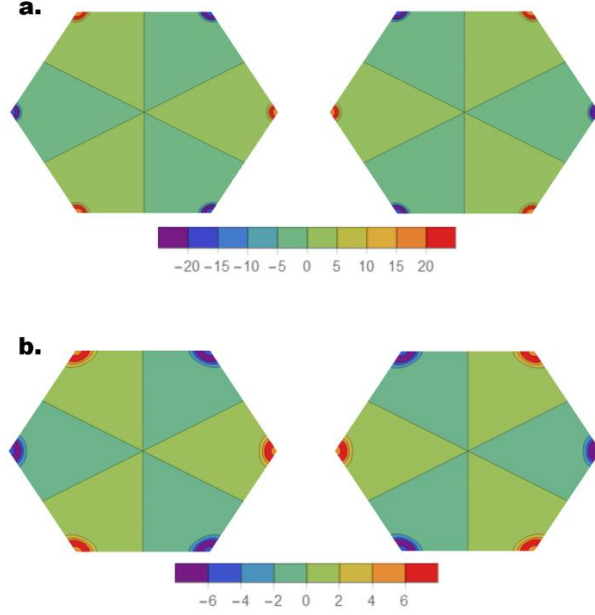


**Figure 4:** (a) and (b) Berry curvatures for the valence-like band  $\epsilon_3$  in AB (left) and BA (right) FBL, with  $(U = 0.2, v_0 = 0.2, D = 0)$  and  $(U = 0.3, v_0 = 0.5, D = 0)$ .

Unlike the DMI case, the Berry curvature has opposite sign near the inequivalent valleys, resulting in zero total Chern number. Nevertheless, integrating the Berry curvature of the valence-like band within the  $\nu K$  valley yields a quantized valley Chern number  $N_\nu = \pm 1$ , in a remarkable analogy with BLG. For a uniform ED potential, reversing the stacking configuration results in a  $\pi/3$  rotation of the Berry curvature, associated with a sign reversal of  $N_\nu$ . The LSW hence separates two distinct topological phases, and induces a topological invariant  $\Delta N_\nu = \pm 2$ . In accordance with the bulk-edge correspondence, a pair of topologically protected valley-polarized chiral magnon modes are expected to flow along the AB-BA interface, with  $\pm K$  valley magnons propagating in opposite directions. This is numerically confirmed in figure 5 for selected values of  $U$  and  $v_0$ . Regardless of the number of the intragap modes localized on the domain wall, there are only two chiral modes per valley, propagating along the 1D channel while preserving the valley index. These results hence constitute a theoretical realization of topologically protected magnon valley transport.

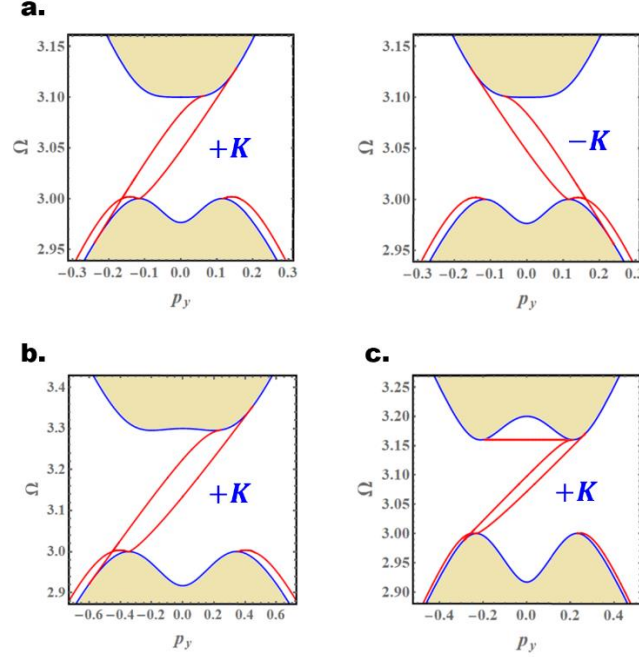


**Figure 5:** (a) Left and right figures respectively show the 1D intragap LSW magnon modes, with 2 chiral modes, near  $\pm K$  valleys. The parameters are ( $U = 0.1$ ,  $D = 0$ ,  $v_0 = 0.2$ ). (b) and (c) show only  $+K$  valley modes for FBL with ( $U = 0.3, D = 0$ ,  $v_0 = 0.5$ ) and ( $U = 0.2$ ,  $D = 0$ ,  $v_0 = 0.2$ ) respectively.

**Discussion.** The inequivalent valleys in the BZ of 2D honeycomb ferromagnets provide an additional degree of freedom for magnons, the valley-index, and its manipulation can lead to novel magnonic devices. Topologically protected magnons are robust against various dissipation sources and are candidates to overcome the difficulty in harnessing the magnon valley degree of freedom in 2D magnets. Here, we demonstrate that LSW in DMI-free FBL can be used to control the valley degree of freedom, giving hope for magnon valleytronic devices based on atomically thin magnetic materials. In particular, we show that magnon valley Chern numbers are well defined, change sign across LSW, and induce 1D topological boundary magnon states. Similar to their fermionic counterpart, the LSW magnon modes have several interesting features that are useful for magnon valleytronics. These modes are gapless and chiral, meaning that their propagation direction along the AB-BA boundary is dictated by the valley-index. The velocity-valley locking and topological protection allows for a long-range ballistic valley transport that conserves the valley-index. These predictions open opportunities to realize magnon valleytronic (nano-)devices, including valley valves, filters, waveguides and transistors. Our study further predicts new topological phases in FBL, as a result of the interplay between ED, DMI and interlayer exchange. Nevertheless, we have concluded that FBL with both ED and DMI are not useful for valleytronic applications. With the rapid advancement in experimental techniques to fabricate and characterize 2D magnetic materials,



experimental testing of our predictions shall be feasible. Already existing candidate materials include ferromagnetic honeycomb chromium compounds like  $CrBr_3$ .

## References

- [1] Gong, C. et al. Discovery of intrinsic ferromagnetism in two-dimensional Van der Waals crystals, *Nature* **546**, 265 (2017).
- [2] Huang B. et al. Layer-dependent ferromagnetism in a Van der Waals crystal down to the monolayer limit, *Nature* **546**, 270 (2017).
- [3] Cheng, R., Okamoto, S. & Xiao, D. Spin Nernst effect of magnons in collinear antiferromagnets, *Phys. Rev. Lett.* **117**, 217202 (2016)
- [4] Zyuzin, V. A. & Kovalev, A. A. Magnon Spin Nernst Effect in Antiferromagnets, *Phys. Rev. Lett.* **117**, 217203 (2016)
- [5] Owerre, S. A. A first theoretical realization of honeycomb topological magnon insulator, *J. Phys.: Condens. Matter* **28**, 386001 (2016)
- [6] Owerre, S. A. Magnon Hall effect in AB-stacked bilayer honeycomb quantum magnets, *Phys. Rev. B* **94**, 094405 (2016)
- [7] Nakata, K., Klinovaja, J. & Loss, D. Magnonic quantum Hall effect and Wiedemann-Franz law, *Phys. Rev. B* **95**, 125429 (2017)
- [8] Shiomi, Y., Takashima, R. and Saitoh, E. Experimental evidence consistent with a magnon Nernst effect in the antiferromagnetic insulator  $MnPS_3$ , *Phys. Rev. B* **96**, 134425 (2017)
- [9] Owerre, S. A. Dirac Magnon Nodal Loops in Quasi-2D Quantum Magnets, *Sci. Rep.* **7**, 6931 (2017)
- [10] Lado, J. L. & Fernández-Rossier, J. On the origin of magnetic anisotropy in two dimensional  $CrI_3$ , *2D Materials* **4**, 035002 (2017).
- [11] Pershoguba, S. S., Banerjee, S., Lashley, J. C., Park, J., Ågren, H., Aeppli, G. & Balatsky, A.V. Dirac magnons in honeycomb ferromagnets, *Phys. Rev. X* **8**, 011010 (2018)
- [12] Lee, K. H., Chung, S. B. Park, K. & Park, J.-G. Magnonic quantum spin Hall state in the zigzag and stripe phases of the antiferromagnetic honeycomb lattice, *Phys. Rev. B* **97**, 180401(R) (2018)
- [13] Jin, W. et al. Raman fingerprint of two terahertz spin wave branches in a two-dimensional honeycomb Ising ferromagnet, *Nat. Comm.* **9**, 5122 (2018)
- [14] Chen, L. et al. Topological spin excitations in honeycomb ferromagnet  $CrI_3$ , *Phys. Rev. X* **8**, 041028 (2018)
- [15] Pantaleón, P. A. & Xian, Y. Effects of edge on-site potential in a honeycomb topological magnon insulator, *J. Phys. Soc. Japan* **87**, 064005 (2018)

- [16] Xing, X. W. et al. Magnon Transport in Quasi-Two-Dimensional van der Waals Antiferromagnets, *Phys. Rev. X* **9**, 011026 (2019)
- [17] Owerre, S. A. Magnonic Floquet Quantum Spin Hall Insulator in Bilayer Collinear Antiferromagnets, *Sci. Rep.* **9**, 7197 (2019)
- [18] Ghader, D. & Khater, A. Discretized dynamics of exchange spin wave bulk and edge modes in honeycomb nanoribbons with armchair edge boundaries, *J. Phys.: Condens. Matter* **31**, 31, 315801 (2019)
- [19] Ghader, D. & Khater, A. Theory for the spin dynamics in ultrathin disordered binary magnetic alloy films: application to cobalt-gadolinium, *JMMM* **482**, 88-98 (2019)
- [20] Ghader, D. & Khater, A. Asymmetric dynamics of edge exchange spin waves in honeycomb nanoribbons with zigzag and bearded edge boundaries, *Sci. Rep.* **9**, 6290 (2019)
- [21] Ghader, D. & Khater, A. A new class of nonreciprocal spin waves on the edges of 2D antiferromagnetic honeycomb nanoribbons, *Sci. Rep.* **9**, 15220 (2019)
- [22] Ghader, D. Magnon magic angles and tunable Hall conductivity in 2D twisted ferromagnetic bilayers, *arXiv:1911.07009* (2019)
- [23] Jiang, S., Li, L., Wang, Z., Mak, K. F., & Shan, J. Controlling magnetism in 2D  $CrI_3$  by electrostatic doping, *Nat. Nanotechnol.* **13**, 549 (2018)
- [24] Zhai, X. & M. Blanter, Y. M. Topological valley transport of gapped Dirac magnons in bilayer ferromagnetic insulators, *arXiv:2002.00446* (2020)
- [25] Rycerz, A., Tworzydło, J. & Beenakker, C. W. J. Valley filter and valley valve in graphene *Nat. Phys.* **3**, 172 (2007)
- [26] Martin, I., Blanter, Y. M. & Morpurgo, A. F. Topological confinement in bilayer graphene, *PRL* **100**, 036804 (2008)
- [27] Zhang, F., MacDonald, A. H. & Mele, E. J. Valley Chern numbers and boundary modes in gapped bilayer graphene, *PNAS* **110**, (26) 10546-10551 (2013)
- [28] Alden, J. S. et al. Strain solitons and topological defects in bilayer graphene, *PNAS* **110**, (28) 11256-11260 (2013)
- [29] Vaezi, A., Liang, Y., Ngai, D. H., Yang, L. & Kim, E.-A. Topological Edge States at a Tilt Boundary in Gated Multilayer Graphene, *Phys. Rev. X* **3**, 021018 (2013)
- [30] Mak, K. F., McGill, K. L., Park, J., & McEuen, P. L. The valley Hall effect in  $MoS_2$  transistors, *Science* **344**, 1489 (2014)
- [31] Xu, X., Yao, W., Xiao, D. & Heinz, T. F. Spin and pseudospins in layered transition metal dichalcogenides, *Nat. Phys.* **10**, **343** (2014)
- [32] Pan, H., Li, Z., Liu, C.-C., Zhu, G., Qiao, Z., & Yao, Y. Valley-polarized quantum anomalous Hall effect in silicene, *Phys. Rev. Lett.* **112**, 106802 (2014)

- [33] Long, J. et al. Topological valley transport at bilayer graphene domain walls, *Nature*, **520**, 650–655 (2015)
- [34] Shaibely, J. R. et al. Valleytronics in 2D materials, *Nat. Rev. Mater.* **1**, 16055 (2016).
- [35] Ang, Y. S., Yang, S. A., Zhang, C., Ma, Z. & Ang, L. K. Valleytronics in merging Dirac cones: all-electric-controlled valley filter, valve, and universal reversible logic gate, *Phys. Rev. B* **96**, 245410 (2017)
- [36] Bussolotti, F. et al. Roadmap on finding chiral valleys: screening 2D materials for valleytronics, *Nano Futures*, **2**, 032001 (2018)
- [37] Vitale, S. A. et al. Valleytronics: opportunities, challenges, and paths forward, *Small* **14**, 1801483 (2018).
- [38] Niu, Z. Spin-valley filter effect and Seebeck effect in a silicene based antiferromagnetic/ferromagnetic junction, *New J. Phys.* **21**, 093044 (2019)
- [39] McCann, E. & Fal’ko, V. I., Landau-level degeneracy and quantum Hall effect in a graphite bilayer, *Phys. Rev. Lett.* **96**, 086805 (2006)
- [40] Ohta, T., Bostwick, A., Seyller, T., Horn, K., & Rotenberg, E. Controlling the electronic structure of bilayer graphene, *Science* **313**, 951–954 (2006)
- [41] Oostinga, J. B., Heersche, H. B., Liu, X., Morpurgo, A. F., & Vandersypen, L. M. K. Gate-induced insulating state in bilayer graphene devices. *Nat Mater* **7**, 151–157 (2008)
- [42] Castro, E. V. et al. Biased bilayer graphene: Semiconductor with a gap tunable by the electric field effect, *Phys Rev Lett* **99**, 216802 (2007)
- [43] Zhang, F., Sahu, B., Min, H., & MacDonald, A. H. Band structure of ABC-stacked graphene trilayers, *Phys Rev B* **82**, 035409 (2010)
- [44] Zhang, F., Jung, J., Fiete, G. A., Niu, Q., & MacDonald, A. H. Spontaneous quantum Hall states in chirally stacked few-layer graphene systems. *Phys Rev Lett* **106**, 156801 (2011)
- [45] Ren, Y., Qiao, Z. & Niu, Q. Topological phases in two-dimensional materials: a review, *Rep. Prog. Phys.* **79**, 066501 (2016)
- [46] Li, J. et al. Gate-controlled topological conducting channels in bilayer graphene. *Nature Nanotech* **11**, 1060–1065 (2016)
- [47] Li J., Morpurgo A. F., Büttiker M., & Martin I. Marginality of bulk-edge correspondence for single-valley Hamiltonians, *Phys Rev B* **82**, 245404 (2010)
- [48] Li, J., Martin, I., Büttiker, M., & Morpurgo, A. F. Topological origin of sub-gap conductance in insulating bilayer graphene, *Nat Phys* **7**, 38–42 (2011)
- [49] Qiao, Z., Jung, J., Niu, Q., & Macdonald, A. H. Electronic highways in bilayer graphene, *Nano Lett* **11**, 3453–3459 (2011)
- [50] Jung, J., Zhang, F., Qiao, Z., & MacDonald, A. H. Valley-Hall kink and edge states in multilayer graphene, *Phys Rev B* **84**, 075418 (2011)

- [51] Zarenia, M., Pereira, J.M., Farias, G. A., & Peeters, F. M. Chiral states in bilayer graphene: Magnetic field dependence and gap opening, *Phys Rev B* **84**, 125451 (2011)
- [52] Yin, L.-J. *et al.* Direct imaging of topological edge states at a bilayer graphene domain wall. *Nat. Commun.* **7**, 11760 (2016)
- [53] Noh, J., Huang, S., Chen, K. P., & Rechtsman, M. C., Observation of Photonic Topological Valley Hall Edge States, *Phys. Rev. Lett.* **120**, 063902 (2018).
- [54] Lu, J., Qiu, C., Deng, W., Huang, X., Li, F., Zhang, F., Chen, S., & Liu, Z., Valley topological phases in bilayer sonic crystals, *Phys. Rev. Lett.* **120**, 116802 (2018)
- [55] Ghader, D., Ashokan, V., Ghantous, M. A. & Khater, A. Spin waves transport across a ferrimagnetically ordered nanojunction of cobalt-gadolinium alloy between cobalt leads, *Eur. Phys. J. B* **86**, 180 (2013)
- [56] Ashokan, V., Ghantous, M. A., Ghader, D. & Khater, A., Ballistic transport of spin waves incident from cobalt leads across cobalt–gadolinium alloy nanojunctions, *JMMM* **363**, 66-76 (2014)
- [57] Ashokan, V., Khater, A., Ghantous, M. A. & Ghader, D. Spin wave ballistic transport properties of  $[Co_{1-c}Gd_c]_{\ell'}[Co]_{\ell}[Co_{1-c}Gd_c]_{\ell'}$  nanojunctions between Co leads, *JMMM* **384**, 18-26 (2015)
- [58] Ashokan, V., Ghantous, M. A., Ghader, D. & Khater, A. Computation of magnons ballistic transport across an ordered magnetic iron-cobalt alloy nanojunction between iron leads, *Thin Solid Films* **616**, 6-16 (2016)
- [59] Khater, A., Saim, L., Tigrine, R. & Ghader, D. Fabry–Perot magnonic ballistic coherent transport across ultrathin ferromagnetic lamellar bcc Ni nanostructures between Fe leads, *Surf. Sci.* **672**, 47 (2018)
- [60] Fukui, T. Hatsugai, Y. & Suzuki, H. Chern numbers in discretized Brillouin zone: efficient method of computing (spin) Hall conductances, *J. Phys. Soc. Jpn.* **74**, 1674 (2005)